Random Tiling and TopologicalDefects in a Two-Dimensional Molecular Network

Matthew O. Blunt,[1] James C. Russell,[1] María del Carmen Giménez-López,[2] Juan P. Garrahan,[1] Xiang Lin,[2] Martin Schröder,[2] Neil R. Champness,[2]* Peter H. Beton[1]*

[1]School of Physics and Astronomy, University of Nottingham, University Park, Nottingham NG7 2RD, UK.
[2]School of Chem-istry, University of Nottingham, University Park, Nottingham NG7 2RD, UK.

*To whom correspondence should be addressed. E-mail: neil.champness@nottingham.ac.uk (N.R.C.); peter.beton@ nottingham.ac.uk (P.H.B.)

ABSTRACT

A molecular network that exhibits critical correlations in the spatial order that is characteristic of a random, entropically stabilized, rhombus tiling is described. Specifically, we report a random tiling formed in a two-dimensional molecular network of *p*-terphenyl-3,5,3′,5′-tetracarboxylic acid adsorbed on graphite. The network is stabilized by hexagonal junctions of three, four, five, or six molecules and may be mapped onto a rhombus tiling in which an ordered array of vertices is embedded within a nonperiodic framework with spatial fluctuations in a local order characteristic of an entropically stabilized phase. We identified a topological defect that can propagate through the network, giving rise to a local reordering of molecular tiles and thus to transitions between quasi-degenerate local minima of a complex energy landscape. We draw parallels between the molecular tiling and dynamically arrested systems, such as glasses.

The tiling of surfaces with simple polygons has fascinated scientists, mathematicians, and artists in both ancient and modern cultures. The mathematical rules that govern the formation of periodic tilings, in which tiles are reg- ularly placed on a surface, have been extensively studied and provide the foundation for the classification of crystalline materials. More recently, the discovery of quasi-crystals has inspired great interest in aperiodic tilings, which exhibit symmetries that are not compatible with translational order (1–5). It is also possible to form tilings in which translational symmetry is absent by using simple tile shapes such as the rhombus with internal angles of 60° and 120°. Rhombus, or lozenge, tilings lead to a particularly rich range of arrangements, which may be periodic, but random nonperiodic tilings are also permitted (6, 7) and have attracted great interest because of their relevance to mixing algorithms (8, 9), antiferromagnetism (10, 11), and entropic models of quasi-crystals (12–15).

We show that a rhombus tiling may be re- alized experimentally in a two-dimensional arrangement of organic molecules adsorbed on graphite. Specifically, we studied the molecule p-terphenyl-3,5,3′,5′ -tetracarboxylic acid (TPTC) (Fig. 1A), which was synthesized as described in (16). The choice of molecule was motivated by the placement of carboxylic acid groups that promote directional intermolecular hydrogen bonding. For TPTC, these groups stabilize two possible relative placements of neighboring molecules, which we refer to as the parallel (Fig. 1B) and arrowhead (Fig. 1C) configurations. Small quantities of a sat- urated solution of TPTC in nonanoic acid were applied to a freshly cleaved highly oriented pyrolytic graphite (HOPG) substrate, and images of the interface between HOPG and the TPTC solu- tion were acquired by using a scanning tunneling microscope (STM) [see (16) for full experimental details]. The samples were prepared and imaged at room temperature. Nonanoic acid has been identified as a suitable solvent by Lackinger et al. (17, 18) in their investigations of trimesic and related acids, and the properties of molecular net- works stabilized by noncovalent interactions such as hydrogen

bonding have been reviewed by a number of authors (19–21). There have also been recent studies of molecules functionalized with multiple carboxylic acid groups, similar to TPTC (22–24).

A typical area of the TPTC network adsorbed on the HOPG surface is shown in Fig. 2A. The terphenyl backbones of the molecules appear as bright rodlike features, and the molecular arrange- ment is unusual because it exhibits hexagonal orientational order but no translational symmetry. The hexagonal order may be discerned from the array of blue dots overlaid on dark contrast fea- tures (corresponding to depressions or pores) in Fig. 2A and, using calibration scans of the graph- ite substrate, we found that the hexagonal array has a period of 16.6 T 0.8 Å oriented at an angle of T6° to the HOPG substrate (16). Although the pores are regularly arranged, the molecular net- work enclosing them is not translationally ordered. Figure 2, B to F, shows that the molecular ar- rangements enclosing different pores (highlighted areas in Fig. 1A) are hexagons formed by a vary- ing number of molecules.

For example, Fig. 2B shows a hexagon formed by three molecules with edges that alternate between a terphenyl backbone and a carboxylic acid– carboxylic acid junction. Figure 2, C and D, shows two alternative hexagonal arrangements formed by the junction of four molecules with two edges formed by the terphenyl backbone. Similarly, the junction in Fig. 2E is formed by five molecules with one terphenyl edge, and the junction in Fig. 2F is formed by six molecules with no terphenyl edges. The lengths of the hydrogen-bonded and terphenyl edges (equivalent to d_1 and d_2 as de- fined in Fig. 1B) are calculated to be 9.6 and 8.7 Å [the intermolecular binding energy E_{HB} = 0.80 eV is calculated to be the same for the parallel and arrowhead arrangements (16)], giving estimated widths of the hexagons in Fig. 2 ranging from 15.8 Å (Fig. 2B) to 16.6 Å (Fig. 2F), which is in good agreement with the measured periodicity. The molecular array shown in Fig. 2A may be built by combining these five structural units in an arrangement that exhibits orientational sym- metry but no translational order.

The network may be mapped onto a tiling by replacing each molecule with a rhombus [see (25) for another example linking molecular arrays to tiling problems]. Each molecule in the network points along one of three high-symmetry directions, and we have chosen, for clarity, to represent these three molecular orientations as rhombi with differ- ent colors. To illustrate the tiling, we have converted each of the hexagonal structural units discussed above into rhombi (Fig. 2). The representations of the junctions in Fig. 2, B to F, correspond to verti- ces where three, four, five, or six rhombi meet. These diagrams also show that, at a molecular level, the mapping is possible because the inter- molecular bonds between neighboring molecules are located at the midpoint of the rhombus edges (Fig. 2G). We suggest that this symmetry is key to identifying other candidate molecules that might form similar networks.

The molecular network displayed in Fig. 2A can be mapped into rhombi, and the resultant tiling is shown in Fig. 2H. The mapping directly accounts for the presence of orientational sym- metry combined with an absence of translational order because the rhombus vertices (pores in the STM images) fall on a hexagonal lattice, even though the arrangement of rhombi is not ordered. Thus, we demonstrate that the molecular array is equivalent to a rhombus tiling.

We also observed tiling defects in the form of triangular voids enclosed completely by rhombi (Fig. 3). These voids are topological defects that occur in two states of effective “charge” corresponding to triangles pointing either “up” or “down” and have been considered theoretically but have not previously been observed (26–28). We observed $\sim 3 \times 10^{-3}$ defects per adsorbed molecule and may unequivocally distinguish these voids from other less intrinsically interesting defects, such as vacancies. The triangular defects have been observed to propagate through the network, as shown in Fig. 3, C to H. This movement results in a rearrangement of a single molecule (or tile) within the network. Figure 3, C and F, shows a comparison of images before and after

such a transition, in which, as expected, effective charge is conserved. The triangular defect under- goes a second movement between Fig. 3, E and G. In our images, this transition appears to be mediated by the temporary presence of an addi- tional species at the defect site, as highlighted in Fig. 3, C and E, possibly an additional TPTC molecule temporarily bound by hydrogen bond- ing. Although it is difficult to determine the exact details of the atomistic mechanism for defect move- ment, this sequence of images shows that defect propagation through the network gives rise to a reordering of molecular tiles and facilitates a tran- sition between different local energy minima.

To determine whether the observed rhombus tilings are ordered or random, we followed pre- vious theoretical studies (10, 12) and introduced an effective height h(x,y) at each vertex (x,y). The height was calculated with the scheme shown in Fig. 4A, in which a displacement along a rhombus edge leads to a change in height of T1. By ar- bitrarily choosing an origin with zero height, it is possible to define h(x, y) for all vertices of a perfect (defect-free) tiling. Within this scheme, a tiling may be visually considered as a perspective of the sur- face of a simple cubic lattice when viewed along a (111) direction. More formally, the rhombus tiling is equivalent to the projection of an irregular sur- face of a three-dimensional simple cubic crystal onto a (111) plane of the cubic lattice. A map of effective height of the STM image (Fig. 2A) is shown in Fig. 4C.

Within the random tiling hypothesis (11), the tilings may be analyzed by introducing an effec- tive free energy G, which, assuming that all vertex types (shown in Fig. 2) are degenerate, is deter- mined entirely by an entropic contribution and is given by G 1/4 ðK$_O$=2Þ∫j∇hj^2 dxdy. This contribu- tion is equivalent to the energy of a deformed surface with elastic constant K$_o$. The gradient ∇h corresponds to the projection in the (x,y) plane of the normal to the representative surface. The tilings that are generated by this free energy have a height representation for which 〈∇h〉 1/4 0, that is, a surface which on average is flat and par allel to a (111) plane of the projected cubic lat-

tice, which is equivalent to a requirement that equal numbers of tiles are oriented in each of the three possible directions. Fluctuations in height with wavevector k are expected with a Fourier spectrum h(k) α K_0^{-1} /κ/$^{-2}$. In two dimensions, this spectrum leads to logarithmic spatial correlations in *h(x,y), C(r)= 〈[h(0)−h(r)]^2〉 = (pK0)$^{-1}$ ln(r)] + c*, where c is a constant and, for o the maximally random rhombus tiling, K$_o$ = p/9 (10, 12).

We calculated the height correlation function C(r) from STM images that had been converted to a height representation (Fig. 4D). The fraction of tiles pointing in the three directions is in the ratio 1:1:1, within statistical error, and thus the condition 〈∇h〉 1/4 0 is satisfied [see (16) for tile maps and ratios of tile orientations]. It is not possible to solely specify h(x,y) in the presence of triangular void defects because the line integral of h(x,y) along a closed path around a triangular void gives a nonzero value corresponding to the winding number of the defect (in this case, T3). However, it is possible to unambiguously calcu- late the contributions to the height correlation function in regions that do not enclose defects. Our method for calculating C(r) is based on this approach and provides reliable data for r ≤ r$_d$, the average defect separation.

As shown in Fig. 4E, the measured C(r) has the expected logarithmic dependence on r, corre- sponding to the critical correlations of a random rhombus tiling (12). The effective elasticity of the tiling may be extracted from the prefactor of the logarithm. We find K$_{eff}$ = 0.58 T 0.03, or equiv- alently K$_{eff}$/K$_o$ ~ 1.7.

The enhancement of the elastic constant over the expected value K$_o$ is explained as a breaking of the exact degeneracy in local bonding arrange- ments, with a small energetic preference for the

arrowhead (Fig. 1C) configuration. This difference in energy results in an energy cost for vertices that have neighboring tiles in the parallel config- uration (Fig. 2, C to E). These vertices [which are not present on the idealized undeformed (111) representative surface, for which molecules are ex- clusively in the arrowhead arrangement (Fig. 4B)] are associated with local changes in height $\nabla h \neq 0$, leading to an energetic contribution to the free energy in addition to the purely entropic term discussed above. These effects lead to an increase in the effective elastic constant K_{eff} in G.

This explanation is consistent with results by Alet et al. (29) for closed packed dimers on the square lattice with aligning interactions, in which there is a critical phase with an effective elasticity that increases with increasing interaction strength D [and an eventual phase transition to an ordered phase for $D \sim kT$ (T, temperature), where other terms become relevant in the free energy G (29)]. In the context of our experiments, D characterizes the energy difference between the parallel and ar- rowhead configurations. Our finding of logarith- mic correlations with K_{eff} close to K_0, to within a factor 2, confirms that our system is in the ran- dom tiling regime and therefore $D < kT$ (0.03 eV). This very small value of energy, comparable with the uncertainty in our calculation of E_{HB}, high- lights the delicate balance required for entropi- cally stabilized randomness in the rhombus tiling.

Although the above analysis of the spatial dis- tribution of tiles is based on the equilibrium free energy G, it is clear that the tilings are frozen, with minimal temporal evolution, in one local min- imum of a complex energy landscape. The sys- tem is dynamically arrested, similar to a glass, and all tile movements are activated with an energy cost that is expected to scale with the number of inter- molecular hydrogen bonds that must be broken. Triangular defects, which mediate the only tile rearrangements that have been experimentally ob- served, have the lowest activation barrier because only three bonds must be broken in order to move a molecule directly adjacent to a defect. Other tile rearrangements, such as the 60° rotation of the hexagonal unit in Fig. 2B, often considered in the context of mixing algorithms for perfect (defect- free) random tilings (8), require six bonds to be broken and would be expected to be exponen- tially suppressed. The observation of the propa- gation of localized defects as a mechanism for transitions between different local energy minima is highly reminiscent of dynamically facilitated mod- els of glass formers (30, 31). Our results demon- strate the potential of molecular tilings as model systems for the study of glasses and provide an interesting alternative to the random molecular networks recently identified by Otero et al. as glassy systems (32).

Our results show that, once formed, tilings are trapped in one of a large number of quasi-degenerate locally stable states that can rearrange through defect migration. Overall, the connection between rhombus tiling and molecular architecture, through the approximate equality $d_1 \sim d_2$, leads to design rules for a general class of analogous molecular networks in two and three dimensions that can provide novel model systems for the study of random structural arrangements and dy- namically arrested materials.

References

1. D. Shechtman, I. Blech, G. Gratias, J. W. Cahn, Phys. Rev. Lett. 53, 1951 (1984).

2. D. Levine, P. J. Steinhardt, Phys. Rev. Lett. 53, 2477 (1984).

3. G. Onoda, P. J. Steinhardt, D. J. DiVincenzo, J. E. S. Socolar, Phys. Rev. Lett. 60, 2653 (1988).

4. J. Ledieu et al., Phys. Rev. Lett. 92, 135507 (2004).

5. J. Yuhara et al., Phys. Rev. B 70, 024203 (2004).

6. M. E. Fisher, Phys. Rev. 124, 1664 (1961).
7. P. Kasteleyn, J. Math. Phys. 4, 287 (1963).
8. D. B. Wilson, Ann. Appl. Probab. 14, 274 (2004).
9. H. Cohn, R. Kenyon, J. Propp, J. Am. Math. Soc. 14, 297 (2001).
10. H. W. J. Blote, H. J. Hilhorst, J. Phys. A 15, L631 (1982).
11. R. Moessner, S. L. Sondhi, E. Fradkin, Phys. Rev. B 65, 024504 (2002).
12. C. L. Henley, in Quasicrystals, the State of the Art, D. P. DiVencenzo, P. J. Steinhardt, Eds. (World Scientific, Singapore, 1999), p. 459.
13. M. Widom, D. P. Deng, C. L. Henley, Phys. Rev. Lett. 63, 310 (1989).
14. N. Destainville, Phys. Rev. Lett. 88, 030601 (2002). 15. A. S. Keys, S. C. Glotzer, Phys. Rev. Lett. 99, 235503 (2007).
16. Materials and methods and additional data are available as supporting material on Science Online.
17. M. Lackinger, S. Griessl, W. A. Heckl, M. Hietschold, G. W. Flynn, Langmuir 21, 4984 (2005).
18. S. J. H. Griessl et al., Langmuir 20, 9403 (2004).
19. S. de Feyter, F. C. de Schryver, J. Phys. Chem. B 109, 4290 (2005).
20. J. V. Barth, G. Costantini, K. Kern, Nature 437, 671 (2005).
21. F. Rosei et al., Prog. Surf. Sci. 71, 95 (2003).
22. H. Zhou et al., J. Am. Chem. Soc. 129, 13774 (2007). 23. M. Blunt et al., Chem. Commun. 2304 (2008).
24. M. Li et al., Angew. Chem. Int. Ed. 47, 6717 (2008). 25. M. Pivetta, M. C. Blum, F. Patthey, W. D. Schneider, Angew. Chem. Int. Ed. 47, 1076 (2008).
26. M. E. Fisher, J. Stephenson, Phys. Rev. 132, 1411 (1963).
27. J. Linde, C. Moore, M. G. Nordahl, Discrete Mathematics and Theoretical Computer Science Proceedings AA (DM-CCG) 23 (2001).
28. W. Krauth, R. Moessner, Phys. Rev. B 67, 064503 (2003).
29. F. Alet et al., Phys. Rev. Lett. 94, 235702 (2005).
30. G. H. Fredrickson, H. C. Andersen, Phys. Rev. Lett. 53, 1244 (1984).
31. J. P. Garrahan, D. Chandler, Proc. Natl. Acad. Sci. U.S.A. 100, 9710 (2003).
32. R. Otero et al., Science 319, 312 (2008).
33. We thank the UK Engineering and Physical Sciences

Research Council (EPSRC) for financial support under grant EP/D048761/01. J.P.G. was supported by EPSRC grant GR/S54074/01. M.S. acknowledges receipt of a Royal Society Wolfson Merit Award.

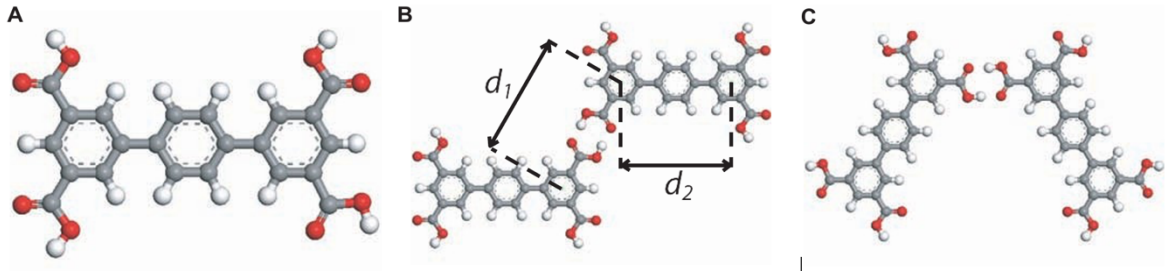

Fig. 1. (A) Molecular structure of TPTC. Two possible arrangements for a pair of TPTC molecules linked via a carboxylic acid–carboxylic acid hy- drogen bond, (B) with the long axes of both molecules parallel to each other, and (C) with one molecule rotated by 60° with respect to the other. Marked on (B) are the calculated distances (16) between two phenyl rings of different TPTC molecules taken across a carboxylic–carboxylic hydrogen bond (d_1), and the distance between the two end phenyl rings of a single TPTC molecule (d_2).

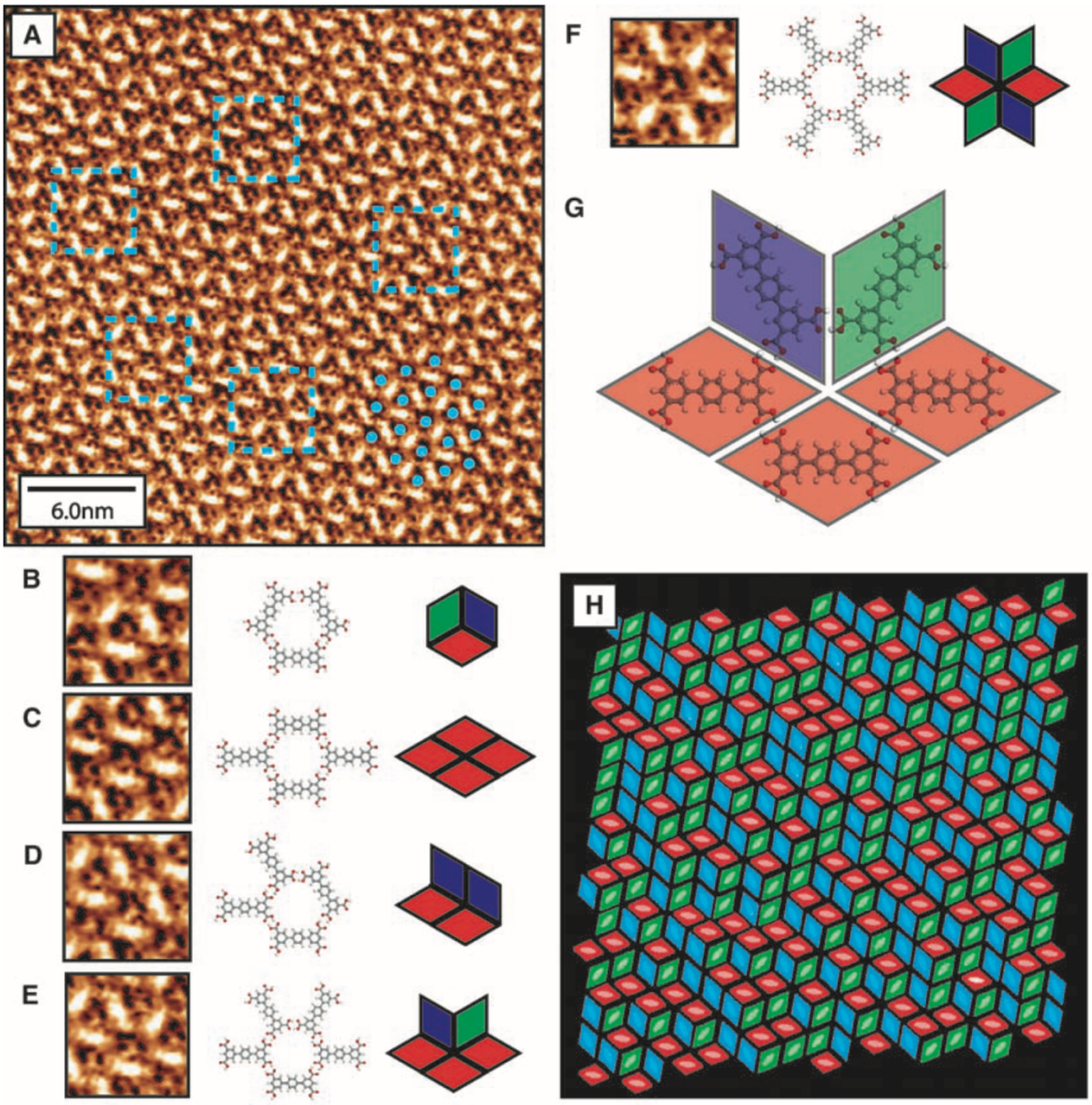

Fig. 2. (A) STM image of a typ- ical area of TPTC network at the nonanoic acid/HOPG interface. The group of three phenyl rings constituting the backbone of the TPTC molecules appear as bright rodlike features in the image. The hexagonal orientational order of the structure is high- lighted by the group of blue dots in the lower right-hand corner of the image, marking the loca- tion of dark contrast regions in the image (depressions/pores in the network). (B to F) Molecular ball and stick diagrams and tiling representations for the five pos- sible arrangements of TPTC mol- ecules around a network pore. Also shown are magnified STM image examples of each pore type from (A); the locations of the magnified regions are marked in (A) by blue dashed squares. Scanning conditions of (A) were tunneling current (I_t) = 0.015 nA and tip voltage (V_t) = 1200 mV. (G) Enlarged version of the mo- lecular arrangement shown in (E). The equivalent tiling representa- tion is shown as a transparent overlay, which highlights the location of the carboxylic acid– carboxylic acid hydrogen bonds at the midpoint of edges between tiles. (H) Corresponding tiling rep- resentation of (A). The coloration of (H) represents the three possi- ble orientations of rhombi within the tiling (red, green, and blue). Idealized representations of the molecular positions are shown faintly in the tiling.

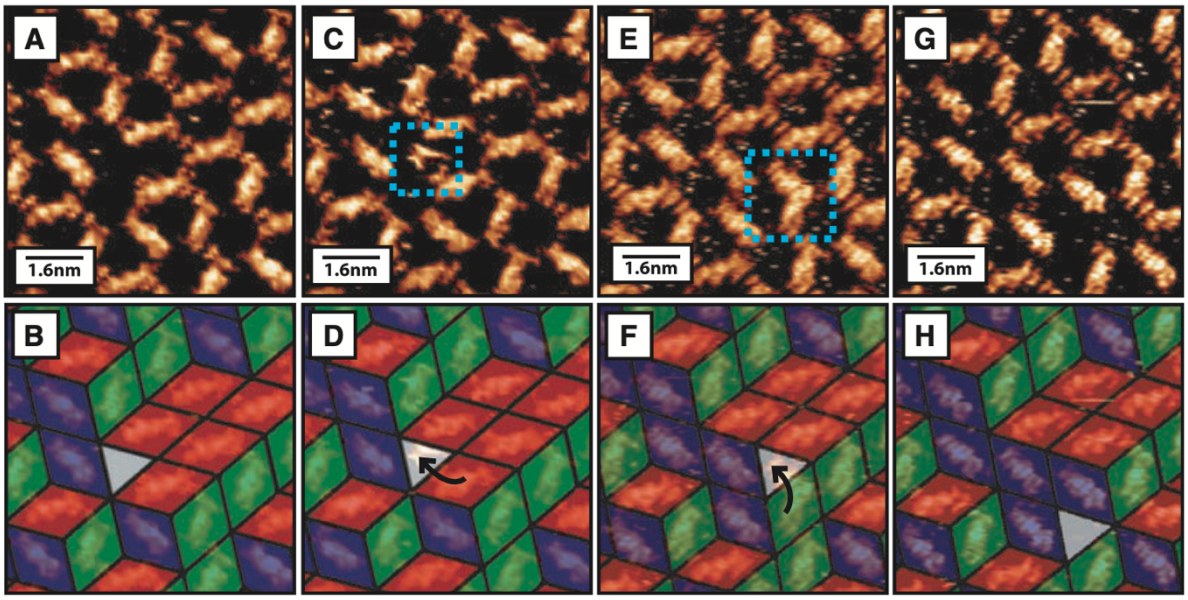

Fig. 3. (A, C, E, and G) STM images showing two separate movements of a single defect through the network structure. (B, D, F, and H) Tiling repre- sentation of the network struc- ture during the defect motion. The effective rearrangements of rhombi in the tiling are marked by the black arrows in (D) and (F). Transient image artifacts observed within the defect site before defect motion are high- lighted by blue dashed squares [(C) and (E)]. Scanning condi- tions for all images were I_t = 0.021 nA and V_t = 1200 mV.

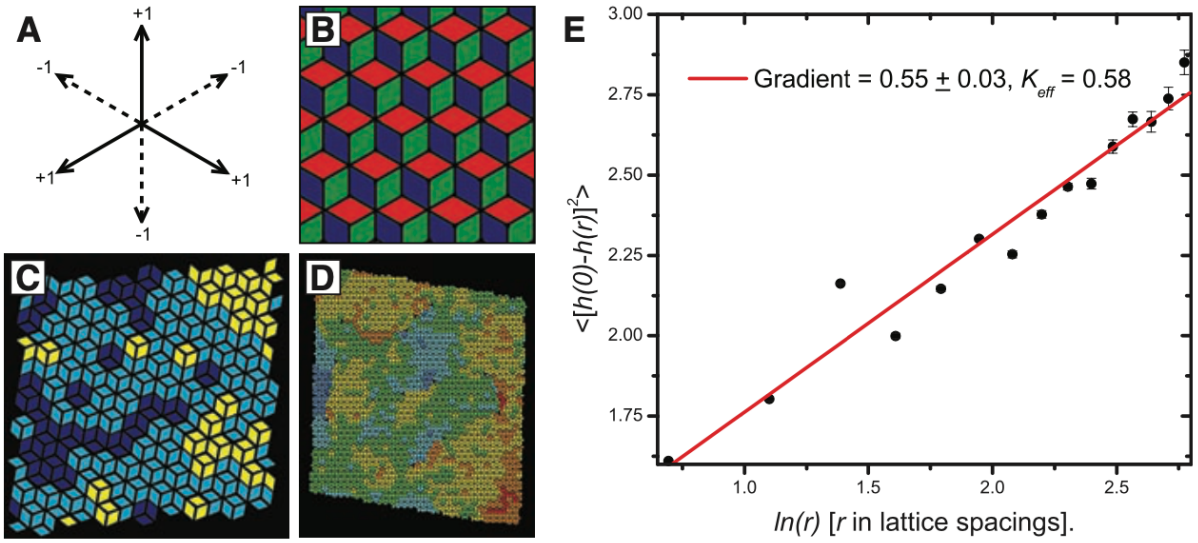

Fig. 4. (A) Scheme for evaluating height function of a tiling. A displacement from a vertex along three of the possible directions leads to an increase in height by 1 as shown; a displacement along the other three directions leads to a decrease by 1. (B) A schematic showing a flat undeformed representative surface to be compared with the (111) surface of a simple cubic crystal. (C) Height representation of tiling in Fig. 2. Here the height of a tile is calculated as the average over its four vertices; different heights are represented as different colors. (D) Height map of one of the large area scans (100 nm by 100 nm) used to generate correlation function [see (16) for more details]. (E) Dependence of correlation on separation demonstrating logarithmic dependence. Scanning conditions for all images were I_t = 0.015 nA and V_t = 1200 mV.

Supporting Online Material for

Random Tiling and Topological Defects in a Two-Dimensional Molecular Network

Matthew O. Blunt[1], James Russell[1], María del Carmen Giménez-López[2], Juan P. Garrahan[1], Xiang Lin[2], Martin Schröder[2], Neil R. Champness[2] & Peter H. Beton[1]

[1] School of Physics and Astronomy, [2]School of Chemistry, University of Nottingham, University Park, Nottingham NG7 2RD, U.K.

Molecular Synthesis

1 was prepared from the oxidation of the methyl groups of 3,5,3',5'-tetramethyl-p-terphenyl, 2, see Scheme 1.

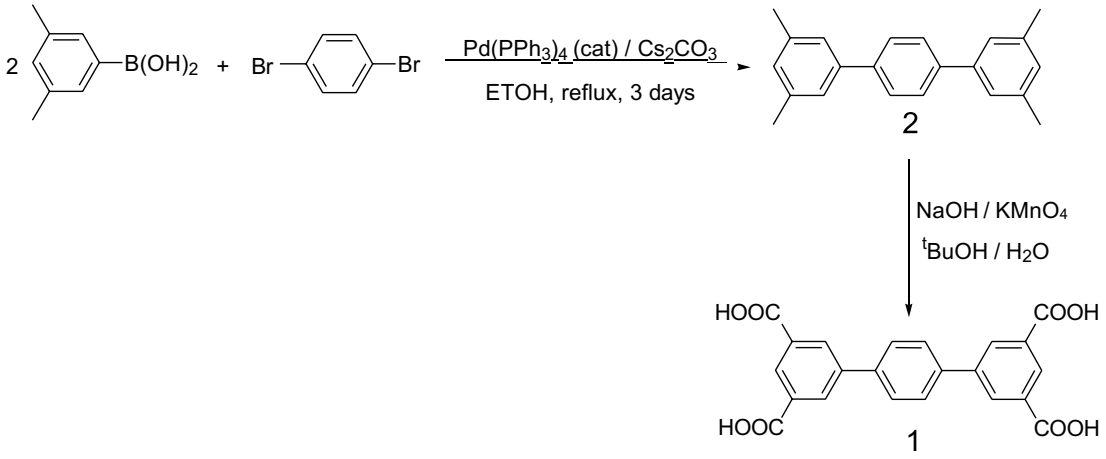

Scheme 1: Suzuki coupling reaction of 2,6-Dibromobenzene with 3,5-dimethylpheylboronic acid follow by oxidation of the methyl groups.

Synthesis of 3,5,3',5'-tetramethyl-p-terphenyl (2)

2,6-Dibromobenzene (378 mg, 1.6 mmol), an excess of 3,5-dimethylphenylboronic acid (600 mg, 4 mmol) and Cs_2CO_3 (1.4 g, 4 mmol) were mixed in ethanol (10 ml), and the mixture was de-aerated using N_2. $Pd(PPh_3)_4$ (18.5 mg, 1% of 1.6 mmol) was

added to the reaction mixture with stirring and the mixture was refluxed to 80°C for 3 days under a N_2 atmosphere. The resultant mixture was evaporated to dryness, extracted into $CHCl_3$ and washed with water. The organic layer was dried over $MgSO_4$ and the solvent was removed under reduced pressure to provide a crude product which was purified by silica gel chromatography using hexane as eluent. The product was obtained as a colourless crystalline solid. Yield: 328 mg, 75%. ^{1}H NMR (acetone-d^6, 270MHz): 7.73 (s, 4H), 7.33(s, 4H), 7.03(s, 2H), 2.38 (s, 12H). ^{13}C NMR (acetone-d^6, 270MHz): δ 140.87, 140.24, 138.37, 129.01, 127.48, 125.05, 21.523. EI-MS (m/z) found: 287.1807 ($[M+H]^+$, 100%). Elemental analysis (% calc/found) for $C_{22}H_{22}$: C 92.26/92.33, H 7.74/7.73.

Synthesis of p-terphenyl-3,5,3',5' -Tetracarboxylic acid (TPTC) (1)

3,5,3',5'-Tetramethyl-p-terphenyl (171 mg, 0.6 mmol) and NaOH (381 mg, 9.5 mmol) were dissolved in *t*-BuOH:water (16 mL, 1:0.6). The reaction was heated to 55°C and an excess of $KMnO_4$ (1.12 g, 7.1 mmol) was added in portions over 2 days. The reaction was kept at this temperature whilst being stirred for two weeks until the oxidation process was completed. A few drops of ethanol were added to the mixture to destroy excess $KMnO_4$. Afterwards, the mixture was heated to 90°C before vacuum filtration to remove MnO_2. The filtrate was concentrated *in vacuo* and concentrated HCl was added dropwise with stirring until no more white precipitated formed (pH=2). The product was collected by centrifugation and washed with water to eliminate excess acid , further washed with acetone and dried in vacuo. Yield: 100 mg, 41 %. ^{1}H NMR (DMSO-d^6, 270MHz): 8.48 (t, 2H, J=1.53 Hz), 8.45 (d, 4H, J=1.53 Hz), 7.92 (s, 4H). ^{13}C NMR (acetone-d^6, 270MHz): δ 167.07, 140.82, 138.73, 132.86, 131.72, 129.58, 128.32. EI-MS (m/z) found: 405.0609 ($[M+H]^-$, 100%), 361.0752 ($[M-H-(COOH)]^-$, 82.6%). Elemental analysis (% calc/found) for $C_{22}H_{14}O_8$: C 65.03/64.95, H 3.47/3.43.

Experimental details

Saturated solutions of TPTC were prepared by mixing approximately 10mg of TPTC with 5ml of nonanoic acid and sonicating for ten minutes. The resulting fine suspension was allowed to settle and the clear solution was decanted from the top. All images were collected using a *Molecular Imaging PicoSPM* using mechanically cut PtIr (90:10) wire, and were taken in solution at the liquid/solid interface. In all the experiments highly orientated pyrolytic graphite substrates (HOPG) were used. The HOPG samples were sonicated in methanol, dried and then mechanically cleaved prior to each experiment. A PTFE liquid cell was used to both hold down the samples during imaging, and to stop the solution escaping.

Image analysis and processing:

In order to eliminate the effects of drift from measurements of the network dimensions the underlying HOPG substrate was used as a calibration. Images were acquired in which parameters were switched from those normally used to image the molecular network to those used for imaging HOPG. The resultant images (see Figure S1) show both the network structure, and the underlying HOPG. By assuming that the rate of drift remains unchanged between the two halves of the image we can use the known lattice constant of graphite to determine the dimensions of the network structure. The pore-to-pore separation for the network structure shown in Figure S1 is 1.66nm $\pm$ 0.08nm, and the hexagonal network of pores is rotated by $6^{o} \pm 1^{o}$ with respect to the underlying HOPG lattice. The value of the pore-to-pore separation is the same, within error, to that reported for a hexagonal network of trimesic acid molecules ~1.7nm [1].

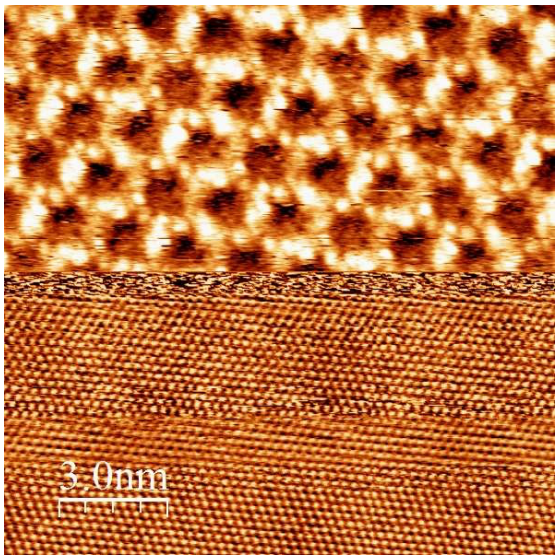

Figure S1: Composite image showing the network structure in the upper section of the image (topography data collected during the forward trace) and the underlying HOPG in the lower section (Current data collected during the forward trace). Imaging parameters, tunnel current: 5pA (top), 1nA (bottom); tip bias: +1.2V (top), +0.1V (bottom).

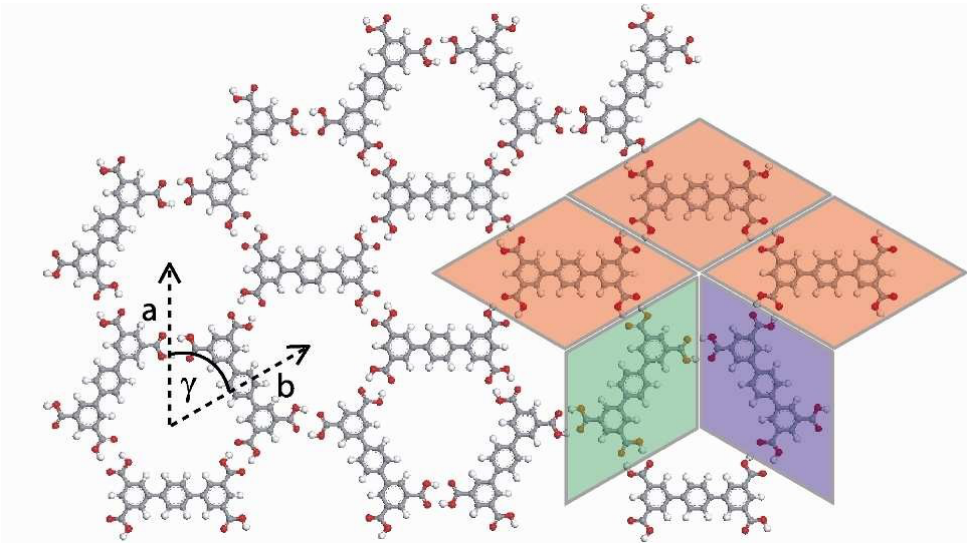

Figure S2: Schematic diagram Showing a random section of TPTC network (a = b = 1.66nm $\pm$ 0.08nm, y = 60° $\pm$ 1°). An overlay displaying a small section of the rhombus tiling for this network is also shown

In order to create the rhombus tilings of STM images drift correction (based on the calibration described above) is performed followed by a conversion to a binary image, and finally the replacement of molecules by tiles to form a tiling (see Figure S2 for a schematic diagram of the tiling process). The tilings produced for the two STM images used in the calculation of the correlation function shown in Figure 4, are displayed in Figure S3.

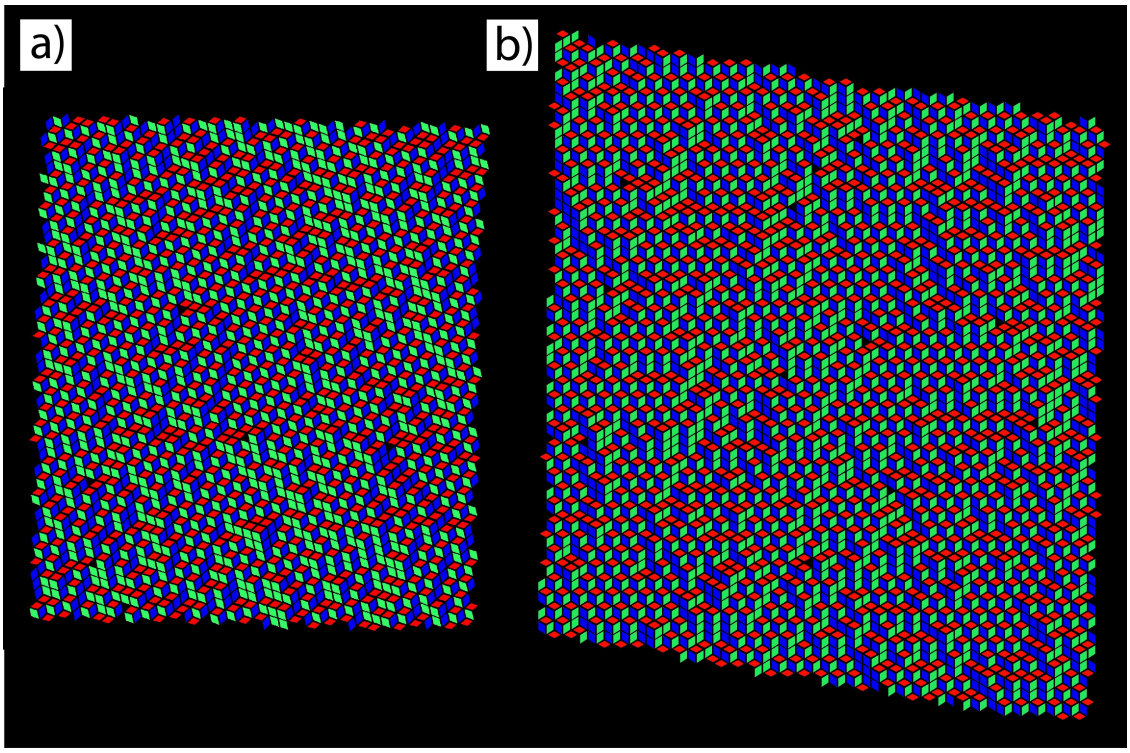

Figure S3: Tilings produced for a) 80nm & b) 100nm STM images taken at different locations on a single sample.

Calculation of Binding Energies and Geometries

All density functional theory (DFT) calculations were carried out using the DMol^3 package in Materials Studio. The generalised gradient approximation functional of Perdew-Burke-Enzerhof was implemented [2]. Core electrons were represented by effective core potentials constructed according to the method of Bergner *et. al.* [3], while double numerical basis sets with polarization functions were used for the valence electrons. The radius within which the atomic orbitals are strictly localized was set to 3.7Å. For geometry optimisations the structure was considered to have converged when the force on the atoms was < 0.1eV Å^{-1}. A default convergence tolerance of 10^{-5} eV was employed for the self-consistent field cycle at each stage of the optimization process.

The stabilization energy associated with a single parallel (E_P) or arrowhead (E_T) carboxylic-carboxylic hydrogen bond was calculated by dividing the total stabilization energies by the number of such bonds giving E_P = -0.80eV and E_T = -0.80eV. The optimized geometry for a single TPTC molecule was found to be planar

without the need to apply any constraints. Following this, the optimized geometries for two different (parallel and arrowhead) arrangements of TPTC molecules were

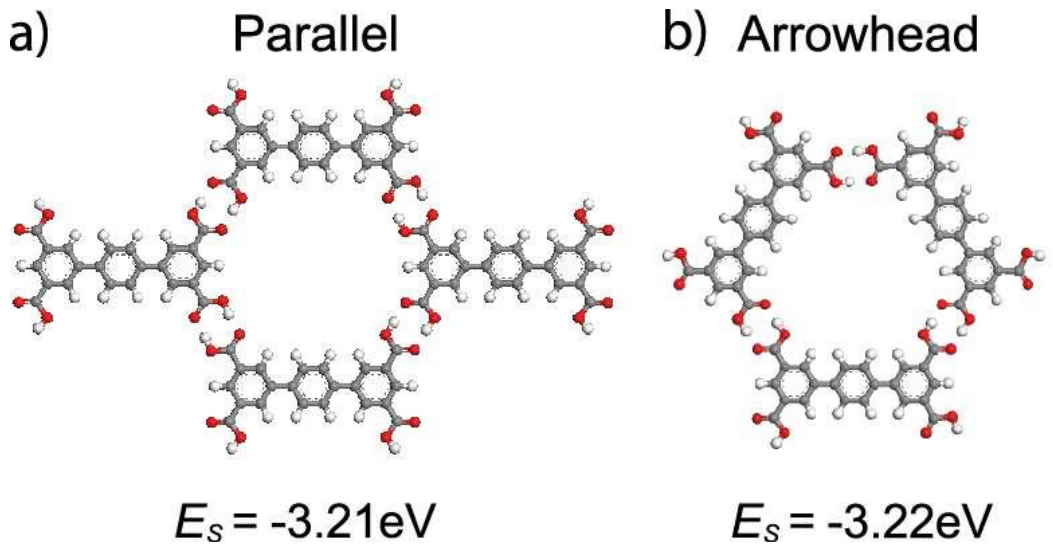

Figure S4: Optimised geometries including total stabilization energies for two different arrangements of TCTP molecules a) parallel and b) arrowhead.

calculated (see Figure S4 a & b). In these simulations the central components of the molecules were constrained to be planar, however the carboxylic acid groups were left unconstrained to allow rotation. Using the energies calculated for the individual molecules the energy gains per molecule due to hydrogen bonding were calculated for the parallel and arrowhead arrangements (see Figure S4a and b).

Tiling Statistics.

The following section details the distribution of tile orientations, number of defects, and defect density for the tilings of the 80nm and 100nm STM images used to generate Figure 4E. The tiling of the 80nm STM image has 2775 tiles in total with 914, 938, and 903 in the three different orientations (33.2%, 34.1%, and 32.8%). The tiling of the 100nm STM image has 4138 tiles in total with 1376, 1383, and 1379 in the three different orientations (33.3%, 33.4%, and 33.3%). The tiling of the 80nm STM image has six defects in total (four of one charge, two of the other) giving a defect density of 2.2×10^{-3}, and an average defect separation of ~20 lattice spacings. The tiling of the 100nm STM image has twelve defects in total (six of one charge, six

of the other) giving a defect density of 2.9×10^{-3}, and an average defect separation of ~17 lattice spacings.

References:

1. M. Lackinger, S. Griessl, W.A. Heckl, M. Hietschold and G.W. Flynn, *Langmuir* 21 4984 (2005).

2. J. P. Perdew, K. Burke, M. Enzerhof, *Phys. Rev. Lett*. 77 3865 (1996).

3. A. Bergner, M. Dolg, W. Kuchle, H. Stoll, H. Preuss, *Mol. Phys.* 80 1431 (1993).